5th Joint International Symposium on Deformation Monitoring (JISDM), 20-22 June 2022, Valencia, Spain
DOI: http://doi.org/10.4995/JISDM2022.2022.13872

Terrestrial Laser Scanning based deformation monitoring for masonry buildings subjected to ground movements induced by underground construction

Yiyan Liu, Sinan Acikgoz, Harvey Burd

Department of Engineering Science, University of Oxford, 15 Parks Road, OX1 3PJ Oxford, United Kingdom, (yiyan.liu@eng.ox.ac.uk; sinan.acikgoz@eng.ox.ac.uk; harvey.burd@eng.ox.ac.uk)

Key words: *Terrestrial Laser Scanning; ground movement; masonry; monitoring; non-rigid iterative closest point (N-ICP)*

ABSTRACT

Tunnelling and deep excavation activities cause ground movements. Monitoring the influence of these ground movements on nearby surface assets is a major component of urban underground construction projects. Such projects often require large-scale and comprehensive monitoring of nearby buildings to track displacements and identify structural damage. Masonry assets are particularly vulnerable to ground movements due to the low tensile strength of the material; these structures may experience unsightly cracking and structural stability issues. Current monitoring practice for these buildings is labour intensive and cannot fully characterise the response of the assets due to the limited number of measurement points. This paper presents a non-contact monitoring solution using terrestrial laser scan (TLS) data, which develops a modified non-rigid iterative closest point (N-ICP) algorithm. This algorithm optimises the displacement fields by establishing point to point correspondences that penalise non-smooth deformations and deviations from landmarks (*i.e*. feature points where displacements are known). The algorithm outputs rich 3D displacement fields that can be used in established assessment and decision-making procedures. To demonstrate this algorithm's ability to estimate 3D displacement fields from point clouds, several synthetic datasets are processed in this study. The results demonstrate the algorithm's potential for recovering underlying deformations with the help of landmarks and optimisation weightings.

I. INTRODUCTION

Urban underground construction requires rigorous and comprehensive monitoring and survey schemes on nearby buildings. For example, Crossrail and High Speed Two require all buildings in risk category 3 (moderate) and above to be monitored from one year prior to construction until the ground movement has ceased (Crossrail Limited, 2008; High Speed Two Limited, 2017). During Crossrail alone, according to Lazarus and Jung (2018), there were approximately 4000 affected buildings along the route, including 300 listed buildings. Instrumenting and monitoring these buildings required expenditure in excess of £60 million (VINCI Construction, 2014).

In underground construction, the monitoring of surface properties forms part of the ground movement control and asset management strategy (British Tunnelling Society, 2011). The monitoring data are used to assess the impact of the ground movements, verify design parameters and models, and inform construction control procedures. The monitoring results are often used as performance indicators for the asset. It is common practice for the main contractor to operate a "traffic light" system so that appropriate actions can be undertaken when "trigger values" are exceeded (Crossrail Limited, 2008; High Speed Two Limited, 2017). Such systems are often at the core of the contractor risk management strategy. Therefore, the reliability and timeliness of the monitoring data are of great importance.

As evidenced in the Jubilee Line Extension (see Burland *et al*., 2001) and the more recent Crossrail projects, the monitoring of surface assets mainly comprises manual monitoring of studs and invar calibrated scales using precise levels and "automatic" monitoring of prisms using total stations. According to Burland *et al*. (2001) and the Tunnel Lining Design Guide published by the British Tunnelling Society (2004), the practical measurement errors of total stations and precise levels can be as high as 0.5 mm. However, the use of precise levels and total stations require the installation of "targets" on the façade. Hence only isolated points can be monitored for movements, and these points may not reflect the response of the building. According to Lazarus and Jung (2018), although extensive monitoring was carried out along tunnel alignments in Crossrail, data collected were often insufficient to understand the behaviour and response of individual buildings to ground movements. Moreover, surveying using precise levels is considered labour intensive.

Point cloud data is a collection of 3D points that represent the external and visible surfaces of 3D

objects, which can be obtained using laser scans or images. The efficient, remote, and contactless data acquisition process generates a dense point cloud that is rich in geometric information. An example of point cloud data of a building façade is shown in Figure 1. Depending on the setup and external factors, the point accuracy of the point cloud obtained from laser scanners or reconstructed from Structure from Motion (SfM) and MultiView Stereo (MVS) techniques is in the order of millimetres. The point accuracy can be as high as one to two millimetres for terrestrial laser scans (TLS) when in the appropriate range (Kersten *et al*., 2021).

In the construction industry, it is common practice to use 3D point cloud data, particularly from laser scans, to create an as-built BIM model upon completion of construction (Wang and Kim, 2019). The data have also been widely used for geometric inspection and construction progress tracking. However, using point cloud data for displacement monitoring is still in its infancy (Mukupa *et al*., 2017). To the best of the authors' knowledge, there is no current standard, specification or guidance on using point cloud data for displacement monitoring. To this end, this paper will first review existing methodologies for displacement analysis using point cloud data before presenting and evaluating their performance with synthetic data.

II. Review of Displacement Analysis Using Point Cloud Data

Due to the advantages of point cloud data mentioned above, various cloud comparison methods have been developed for displacement analysis, including Cloud-to-Cloud (C2C) comparison, Cloud-to-Mesh (C2M) comparison and Multiscale Model to Model Cloud Comparison (M3C2), which have been comprehensively reviewed in Lague *et al*. (2013). The displacement models and characteristics of these methods are summarised below.

A. *Cloud-to-Cloud comparison (C2C)*

C2C method establishes point correspondence between two-point clouds based on the Euclidean distance between points. The same idea was used in the popular iterative closest point algorithm proposed by Besl and McKay (1992). The point in the deformed point cloud, which has the closest distance to a point in the undeformed point cloud, is chosen as its corresponding point. The displacement is calculated as the difference in coordinates between these corresponding point pairs.

This method is the simplest and fastest method for cloud comparison as it does not require calculating surface normals or meshing. However, the method is sensitive to measurement noise (Lague *et al*., 2013) and point density (Mukupa *et al*., 2017). More importantly, when used for relatively complex geometries, *e.g*. a curved surface, the correspondence established by the closest point method is influenced significantly by point cloud and deformation geometry. In such cases, the closest distances between point clouds are not representative of deformations and can result in erroneous displacement interpretations (Acikgoz *et al*., 2017). Examples of the use of the C2C method for displacement analysis include Jafari *et al*. (2017) and Gawronek *et al*. (2019).

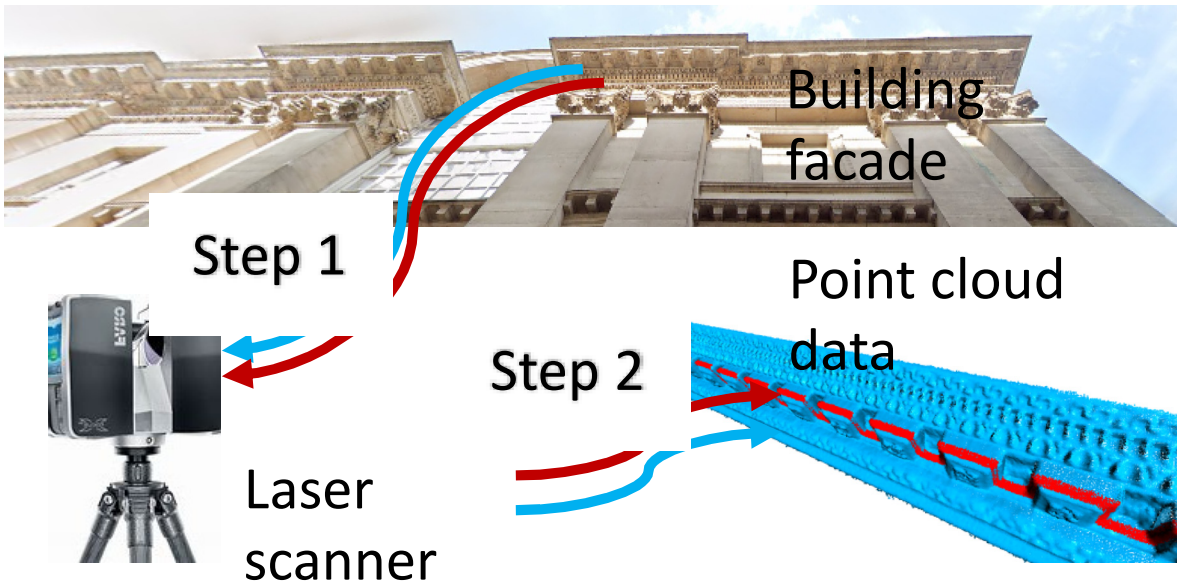

Figure 1. Acquisition of point cloud data of the building façade at Mansion House using a laser scanner. The details of façade ornaments are preserved in the point cloud. Two scans obtained at two different states shown as red and blue point clouds aligned together. For illustration purposes, only part of the red point cloud is shown. The image of Mansion House east façade was extracted from Google Street View. The image of the Faro X330 laser scanner was extracted from image.bing.com under a creative commons license.

B. *Cloud-to-Mesh comparison (C2M)*

C2M method defines the point displacement as the distance between a point in the undeformed point cloud and the nearest element of the mesh of the deformed point cloud along its surface normal. This method requires meshing of the deformed cloud and searching for the nearest mesh element, which is computationally expensive. The method works well on out-of-plane displacements of flat surfaces (Lague *et al*., 2013), but since the true correspondence between points and mesh vertices is not established, the in-plane displacements are challenging to identify. Examples of the use of the C2M method for displacement analysis include Caudal *et al*. (2017) and Mugnai *et al*. (2019).

C. *Multiscale Model to Model Cloud Comparison (M3C2)*

M3C2 method involves selecting core points in the deformed cloud, constructing a cylinder through each core point in a specified direction and calculating the average distance between points in both point clouds in the cylinder along the predefined direction. The M3C2 method is useful for determining displacements of flat surfaces and minimising the influence of measurement noise on displacement estimations. However, like C2C and C2M methods, the arbitrary nature of determining correspondences in M3C2 may lead to inaccurate deformation estimates (Acikgoz *et al*., 2017). While the method provides reasonable estimates for out of plane deformations of flat surfaces (Acikgoz *et al*., 2021), it can struggle with complex geometries and in-plane displacements. Examples of the use of the M3C2 method for displacement analysis include Jafari *et al*. (2017) and Acikgoz *et al*. (2017).

III. Optimal step Non-rigid ICP (N-ICP) algorithm

The optimal step N-ICP algorithm was proposed by Amberg *et al*. (2007). It is a point cloud registration algorithm which aims to find the optimal affine transformation for each vertex of a point cloud that deforms it to corresponding points in another point cloud subject to stiffness and landmark constraints. The N-ICP algorithm, and its predecessor proposed by Allen *et al*. (2003), were originally intended to register templates to human face or body scans while allowing the template to deform.

The N-ICP algorithm is a popular point cloud registration algorithm in the computer vision community and is capable of registering point clouds of complex geometry with small reconstruction errors. To the best of our knowledge, the algorithm has not been used for displacement analysis in structural health monitoring. It has the potential to address issues with existing cloud comparison methods reviewed in Section II because: (i) the displacement of each vertex can be recovered by the non-rigid registration of two point clouds; (ii) the number of degree-of-freedom for each vertex and the use of stiffness constraints are compatible with the physics of deformation; (iii) with the additional landmark constraints, the algorithm has a mechanism to control the optimisation path and capture true point correspondences. A schematic of the N-ICP algorithm is shown in Figure 2 below.

The N-ICP algorithm, in essence, solves the optimisation problem for the cost function (Eq. 1):

$$\bar{E}(X) = \bar{E}_d(X) + \alpha\,\bar{E}_s(X) + \beta\,\bar{E}_l(X) \qquad (1)$$

where $\bar{E}(X)$ is the cost function; $\bar{E}_d(X)$ is the distance term; $\bar{E}_s(X)$ is the stiffness term; $\bar{E}_l(X)$ is the landmark term; α, β are stiffness and landmark weightings, respectively; X is the transformation matrix for the source cloud. Through minimising the cost function with the optimal transformation X, the best affine transformation for each vertex can be obtained under fixed stiffness and landmark weightings. At each step, a new correspondence is determined through the closest point search.

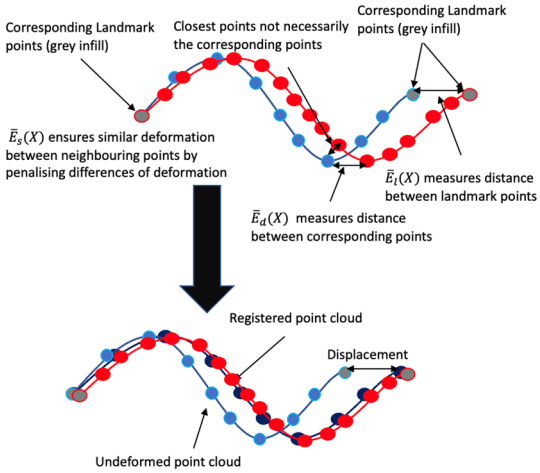

Figure 2. A schematic of the N-ICP algorithm. Displacements are recovered by registering the undeformed point cloud (blue point cloud) to the deformed point cloud (red point cloud). Landmark points are marked with grey infill in both undeformed and deformed point clouds. The registered point cloud after N-ICP is shown in dark blue in the bottom. Registration errors (the difference between dark blue points and red points) are exaggerated for illustration purposes.

However, it is not possible to know the optimal stiffness α beforehand. A high value of α leads to a globally affine transformation, which may be suitable for early algorithm steps to capture gross rigid body movements. A small value of α leads to non-rigid deformations, which may be suitable for consecutive steps to minimise the distance between point clouds. Following this logic, Amberg *et al*. (2007) introduced iterative steps to find a globally optimal solution.

With this setup, a list of stiffness values is used over a for-loop. The stiffness values start from high value to ensure global registration and gradually reduce to allow more localised deformation. For each stiffness value, the best affine transformation is determined by

minimising the cost function in Equation 1. The solution is then used to update the undeformed point cloud before undertaking the closest point search again. Based on the new correspondence, another minimisation is conducted. This iteration is repeated until the Frobenius norm of the difference between the two most recent transformation matrices is below a threshold, *i.e.*, the change in deformation is too small, and no new correspondences are found.

Similar to stiffness weights, Amberg *et al.* (2007) recommended the use of a series of decreasing landmark weights to account for inaccuracies associated with landmark correspondence. However, it is not clear from the paper how the initial landmark weight is determined. In the implementation and evaluation below, an additional dynamic mechanism to determine the landmark weighting β based on the ratio of landmark term and distance terms in Equation 1 is introduced. This is used to prioritise landmark registration at the beginning of the iteration as (Eq. 2):

$$\beta = 1.5 \times \frac{\bar{E}_d(X)}{\bar{E}_l(X)} \quad (2)$$

where $\bar{E}_d(X)$ is determined by the original point coordinates of the undeformed cloud and corresponding points in the deformed point cloud; $\bar{E}_l(X)$ is determined by the original coordinates of selected landmark points in the deformed and undeformed point clouds. Before registration, there is no deformation, the stiffness term is zero, therefore, not included in the above determination.

IV. Experiment Setup

The façade under consideration here is 2 m long and 1 m wide, as shown in Figure 3a. Two point clouds of the main plane of the façade are simulated by two sets of 20,000 randomly generated points (through the generation of 20,000 uniformly distributed float numbers between 0 and 1, and scaled by the length and width, respectively), which are used to account for the correspondence uncertainty. The measurement errors associated with point positions due to laser scan single point accuracy is referred to as measurement noise and is simulated by a random number between 0 to 0.002 (uniformly distributed) in metre unit. This random number describes each point's *z* coordinate. Four "extrusions" that have a size of 0.25 × 0.2 × 0.1 m and are of the same point density as the main plane are added to simulate common features, *i.e.*, exterior elements, ornaments and finishes on the building facades.

This study considers “in-plane” deformation and “out-of-plane” deformation as two basic deformation patterns, which are commonly observed in field monitoring. "In-plane" and "out-of-plane" deformations are defined in relation to the main plane of the façade in the *xy* plane. The displacement field is added to one of the point clouds while another point cloud is used as the undeformed cloud. By taking these two point clouds as inputs, the results from the N-ICP algorithm, C2C, C2M and M3C2, are compared to the known displacement field to assess their relative performance. Benchmark C2C, C2M and M3C2 cloud comparison methods are performed using the software CloudCompare. Bespoke software was written in Python to implement N-ICP. For N-ICP, unless otherwise stated, a list of 10 stiffness weighting ranging from 10000 to 1 is used. Landmarks are used for some examples. When in use, the landmark weighting is determined in accordance with Equation 2.

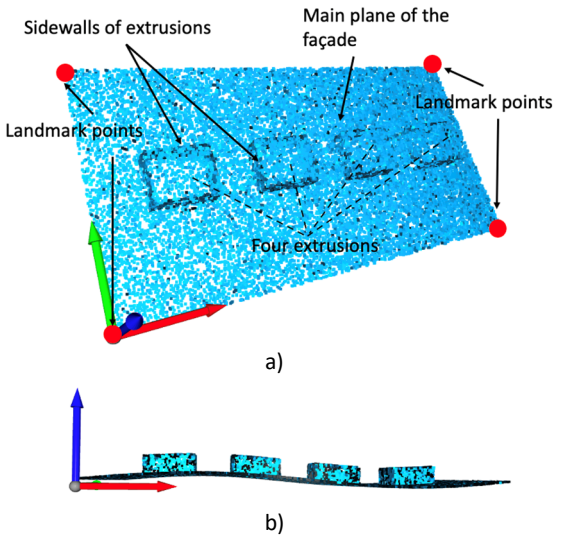

Figure 3. a) Synthetic façade considered in this study; b) Deformed point cloud subjected to “out-of-plane” deformation (Deformation exaggerated for illustration purpose) (Red, green, blue arrows indicate x, y, z directions respectively).

In the following discussion, the point normal refers to the surface normal of a local region represented by that point and its neighbouring points. The points that form the sidewall of the extrusions on the façade, as shown in Figure 3a, have their point normal significantly different to the point normal of the main plane of the façade. These points are referred to as feature points.

V. Discussion of Results

A. *Façade subjected to out-of-plane displacement*

A sine displacement is added to the z direction (as indicated by the blue arrow shown in Figure 3a) of the point cloud as a function of the x coordinate (coordinate direction along the façade as indicated by the red arrow in Figure 3a). The out-of-plane displacement d_z has a maximum value of 5mm and is defined as (Eq. 3):

$$d_z = 0.005 \times sin(\pi x) \quad (3)$$

For the simple out-of-plane displacement case, C2C, C2M, M3C2 and N-ICP all capture the small displacement reasonably well, as shown in Figure 4a.

The relative performance of C2C, C2M, M3C2 and N-ICP can be further assessed by computing their standard deviations from true values using (Eq. 4):

$$\sigma = \sqrt{\frac{1}{n}\sum_{i=1}^{n}(d_i - d_i^t)^2} \quad (4)$$

where σ is the standard deviation from true values and referred to as the error index in the text below, and its units (m) are omitted for brevity; d_i is the measured displacement; d_i^t is the true displacement from the displacement field in Equation 3; n is the number of measurements.

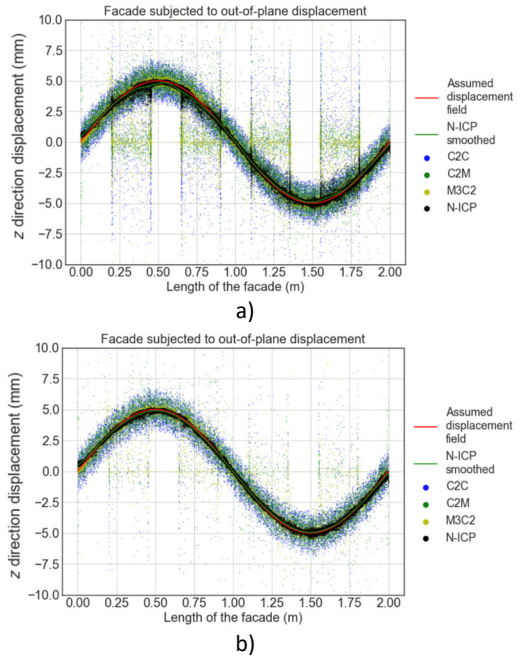

Figure 4. Comparison of out-of-plane displacement analysis of a façade using N-ICP with benchmark methods C2C, C2M and M3C2. (a: all points used in the analysis; b: feature points removed).

The error indices of C2C, C2M, M3C2 and N-ICP are $\sigma_{c2c} = 2.23 \times 10^{-3}, \sigma_{c2m} = 2.04 \times 10^{-3}, \sigma_{m3c2} = 3.78 \times 10^{-3}$, $\sigma_{N-ICP} = 0.52 \times 10^{-3}$ respectively, as illustrated in Figure 4a. N-ICP has a considerably smaller error index compared to other methods.

The majority of errors associated with C2C, C2M and M3C2 are due to the feature points, whose point normals are not along the *z* direction. The feature points are either in the *xz* or *yz* plane; therefore, the displacement along the *z* direction is, in fact, "in-plane" displacement. The C2C, C2M and M3C2 algorithms struggle with such displacements. If the feature points are filtered out by setting a normal threshold, the errors reduce considerably, as shown in Figure 4b. The error indices of C2C, C2M, M3C2 and N-ICP become $\sigma_{c2c} = 1.42 \times 10^{-3}$, $\sigma_{c2m} = 1.58 \times 10^{-3}$, $\sigma_{m3c2} = 2.79 \times 10^{-3}$, $\sigma_{N-ICP} = 0.26 \times 10^{-3}$ respectively.

The uniformly distributed measurement noise in *z* direction is bounded by 0 and 0.002. The standard deviation of the noise is 0.58×10^{-3}. For out-of-plane displacements, the N-ICP algorithm manages to reduce the error index below the standard deviation of the measurement noise. If a locally estimated scatterplot smoothing is applied to the N-ICP results, as shown in Figure 5a, the performance can be further improved to $\sigma_{N-ICP\_Smoothed} = 6.70 \times 10^{-5}$.

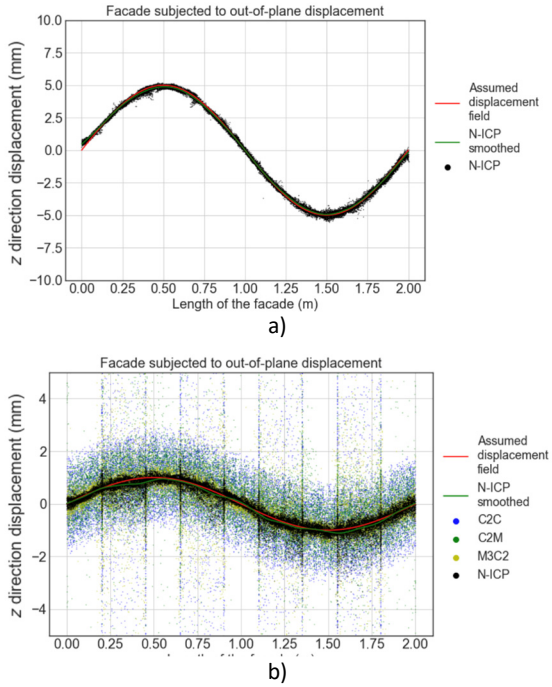

Figure 5. a) Assumed displacement $d_z = 0.005 \times sin(\pi x)$ – Performance of N-ICP further enhanced by using locally estimated scatterplot smoothing(out-of-plane displacement only); b) Assumed displacement $d_z = 0.001 \times sin(\pi x)$ - Comparison of out-of-plane displacement analysis of a façade using N-ICP with benchmark methods C2C, C2M and M3C2.

When the introduced out-of-plane displacement is within the range of measurement noise, *i.e.*, $d_z = 0.001 \times sin(\pi x)$ as shown in Figure 5b, N-ICP continues to perform well. The error indices of N-ICP and N-ICP smoothed are 0.51×10^{-3} and 8.03×10^{-5}, compared to 1.73×10^{-3} for C2C, 1.67×10^{-3} for C2M and 2.41×10^{-3} for M3C2. The error indices of M3C2, C2C and C2M are all substantially greater than the introduced maximum displacement, while the error index for N-ICP remains less than the standard deviation of the measurement noise.

This example demonstrates that for the analysis of a façade subjected to out-of-plane displacement: (i) N-ICP outperforms C2C, C2M and M3C2; (ii) for small displacements, the relatively large error indices of C2C, C2M and M3C2 may invalidate displacement estimations whereas N-ICP can recover accurate displacement fields after smoothing when the measurement noise is uniformly distributed.

The ability of N-ICP to recover small displacements within the range of measurement noise is an important property as it puts less stringent requirements on laser scan single point accuracy.

B. *Façade subjected to in-plane displacement*

For in-plane displacement analysis, a quadratic displacement is added to the *y* direction of the point cloud (as indicated by the green arrow shown in Figure 6a) as a function of the x coordinate (Eq. 5):

$$d_y = -0.01\,x^2 \tag{5}$$

Without using any landmarks, N-ICP successfully captures the trend of the displacements (see Figure 6b). However, at both ends of the façade, the displacement diverges from the true values. For *x* values between 0 m to 0.2 m and 1.8 m to 2 m, there are no features, and N-ICP finds an "optimum" solution primarily based on closest point correspondence; this yields erroneous displacement estimates. On the other hand, C2C cannot detect meaningful in-plane displacement along the *y* direction except for some points at the extrusions. M3C2 also picks up some displacement at the features but, overall, fails to capture the displacement pattern.

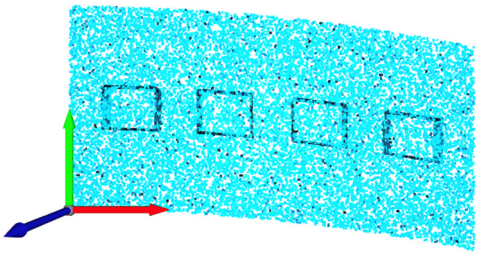

a)

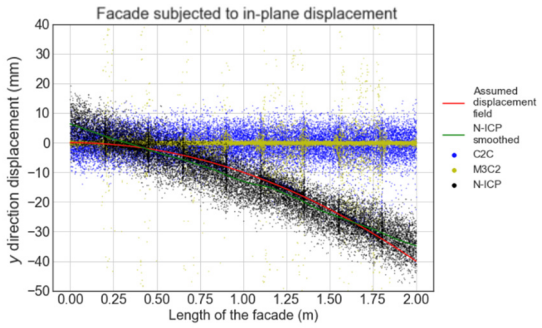

b)

Figure 6. a) Point cloud subjected to "in-plane" deformation along the y direction (Deformation exaggerated for illustration purpose; Red, green, blue arrows indicate x, y, z directions respectively); b) Comparison of in-plane displacement analysis of the façade using N-ICP with C2C and M3C2.

The error index of N-ICP in Figure 6b is 4.8×10^{-3}, which is significantly greater than the out-of-plane case. However, the performance of N-ICP is still much better than C2C and M3C2, whose error indices are in excess of 1.70×10^{-2}.

To understand the increased error index of N-ICP, analyses of two point clouds of the 2m by 1m façade subjected to no displacement field are conducted. For the 2 m by 1 m façade, two sets of 20,000 (Case 1) or 200,000 (Case 2) uniformly distributed random points were generated, and the differences of the *x* coordinates of closest points between the two sets of points were determined as shown in Figure 7. The normalised count numbers in Figure 7 are the raw counts of points within a specific interval divided by the total point number and the width of the selected interval so that the total area under the histogram is unity. The analyses in Figure 7 were undertaken using the *x* coordinate, but the *y* coordinate could also have been used. This difference in *x* coordinates of the two closest points is seen as a potential source of error for displacement analysis, which is intrinsic to the point density of the point cloud. With 200,000 points over the same façade, the error index (standard deviation of the difference in *x* coordinates) has reduced from 4×10^{-3} in Figure 7a to 1.3×10^{-3} in Figure 7b.

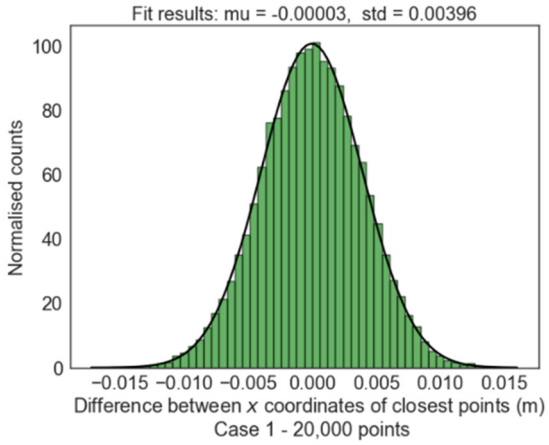

a)

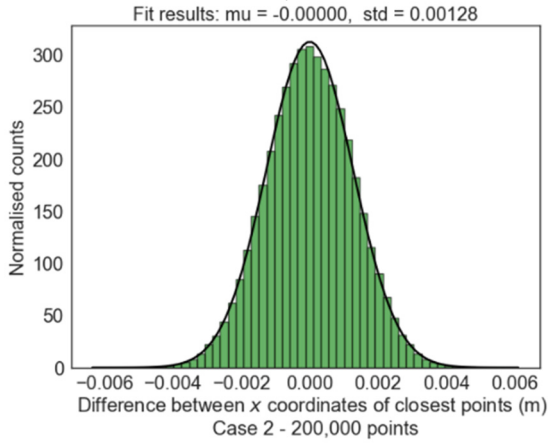

b)

Figure 7. Distributions of x coordinate differences between closest points: a) Case 1 – 20,000 points; b) Case 2 – 200,000 points.

By comparing the error indices associated with N-ICP data in Figure 6b (4.8×10^{-3}) and Figure 7a (4×10^{-3}), it is noted that the error index of N-ICP for in-plane displacement is similar to the error index that

is obtained when the displacements of undeformed point clouds are evaluated. This indicates that the error index of N-ICP is significantly influenced by the point density, *e.g.* the *x* coordinate differences of closest point sets.

It is worth noting that the sensitivity of the error index due to point density can be mitigated by smoothing if the point cloud is of even density. For the case where the façade is subjected to $d_y = -0.01\,x^2$, the error index of smoothed N-ICP results become 2.33×10^{-3} (see Figure 6b).

How the measurement error indices vary with the amplitude of the displacement field can also be investigated. Suppose the façade is subjected to $d_y = -0.001\,x^2$ and $d_y = -0.005\,x^2$. The corresponding error indices of N-ICP become 3.70×10^{-3} and 4.24×10^{-3}, respectively. In the above examples, the error indices remain in the same order of magnitude despite an increase in the maximum displacement from 4 mm to 20 mm. As such, for in-plane displacements smaller than the point spacing, it would be difficult to distinguish displacement from the background noise.

The performance of N-ICP can be further enhanced by using landmark terms. Four corner points of the rectangular façade are selected as landmarks (as indicated in Figure 3a), and passed in as inputs. As a consequence, the error index of N-ICP reduces from 4.82×10^{-3} in Figure 6b (where landmarks were not used) to 4.44×10^{-3} in Figure 8b. It can be seen that sections between features, *i.e.*, the section between 0.20 to 0.45 m and 0.65 m to 0.90 m in *x* direction, as shown in Figure 8, have the largest errors. Points where features are located and whose normal is along the displacement direction (Figure 8a) have the most reliable results.

In summary, we have shown that for the examined in-plane deformation: (i) C2C and M3C2 cannot capture displacements except at specific locations, (ii) without the landmark term, N-ICP can recover the displacement of the entire façade using available features; (iii) in the absence of features or landmarks, N-ICP primarily uses closest points to establish the correspondence and this may lead to erroneous results; (iii) N-ICP's performance can be enhanced by using the landmark term; (iv) the in-plane measurement accuracy of N-ICP depends on the point density and this can be mitigated using smoothing.

VI. Summary

This paper evaluated the performance of several point cloud comparison techniques previously used to estimate deformations. Synthetic point clouds of predominantly planar surfaces, inspired by façades, were generated and deformed in a non-rigid manner. The known deformation fields were compared to deformations estimated by four different algorithms, including a modified version of the non-rigid iterative point cloud algorithm, N-ICP. This algorithm outperforms the other examined techniques (C2C, C2M and M3C2 algorithms). Sources of errors for the N-ICP algorithm are analysed for different deformation scenarios, and the accuracy of the algorithm is quantified using simple statistical measures. The results demonstrate that this algorithm can achieve deformation estimates with smaller errors than the single point measurement accuracy of the point cloud, particularly for displacements in the out-of-plane direction. Compared to out-of-plane displacements, the proposed method predicts in-plane displacements with a greater error margin. The errors are particularly influenced by the point density of the point cloud. However, the algorithm is able to accurately estimate in-plane displacements when landmarks are used, and feature points constrain the registration.

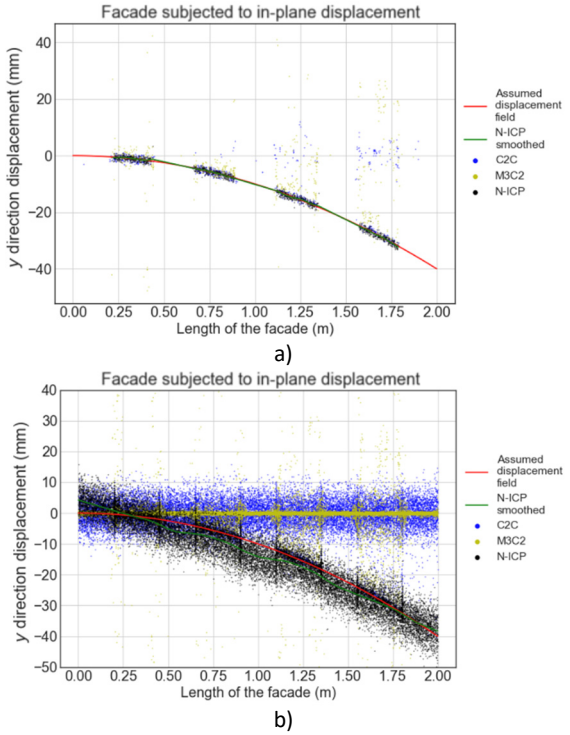

Figure 8. N-ICP performance for in-plane displacement analysis with the use of landmarks: (a) displacement of points in the *xz* plane; b) all points used in the analysis.

Deformations of buildings subjected to ground movements due to underground construction works include both in-plane and out-of-plane displacements. To obtain accurate displacement results using the proposed N-ICP algorithm in field applications would require establishing reliable landmark correspondence. Furthermore, stiffness weightings used in the current N-ICP algorithm are not based on material properties and are determined somewhat arbitrarily. Further research by the authors will aim to address these issues to support the use of point cloud monitoring in future applications.

VII. ACKNOWLEDGEMENTS

This research was funded by the Engineering and Physical Sciences Research Council (EPSRC) of the United Kingdom and Arup Group Ltd through the iCASE project (Project Reference: 2280800).

References

Acikgoz, S., Luciano, A., Dewhirst, M., Dejong, M.J., and Mair, R., (2021). Innovative monitoring of the response of a heritage masonry building to nearby tunnelling in London Clay. *Géotechnique*, pp. 1–16.

Acikgoz, S., Soga, K., and Woodhams, J., (2017). Evaluation of the response of a vaulted masonry structure to differential settlements using point cloud data and limit analyses. *Constr. Build. Mater*. 150, pp. 916–931.

Allen, B., Curless, B., and Popović, Z., (2003). The space of human body shapes: Reconstruction and parameterization from range scans. *ACM Trans. Graph*. 22, pp. 587–594.

Amberg, B., Romdhani, S., and Vetter, T., (2007). Optimal Step Nonrigid ICP Algorithms for Surface Registration. In: 2007 *IEEE Conference on Computer Vision and Pattern Recognition*, pp. 1–8.

Besl, P.J., and McKay, N.D., (1992). A method for registration of 3-D shapes. *IEEE Trans. Pattern Anal. Mach. Intell*. ,14, pp. 239–256.

British Tunnelling Society (2004). *Tunnel lining design guide, Tunnel lining design guide*. Thomas Telford Ltd, London.

British Tunnelling Society (2011). *Monitoring Underground Construction*, ICE Publishing. Thomas Telford Ltd, London.

Caudal, P., Grenon, M., Turmel, D., Locat, J., (2017). Analysis of a Large Rock Slope Failure on the East Wall of the LAB Chrysotile Mine in Canada: LiDAR Monitoring and Displacement Analyses. *Rock Mech. Rock Eng*. 50, pp. 807–824.

Crossrail Limited (2008). Crossrail Information Paper D12 – Ground Settlement [WWW Document]. URL http://74f85f59f39b887b696f-ab656259048fb93837ecc0ecbcf0c557.r23.cf3.rackcdn.com/assets/library/document/d/original/d12groundsettlement.pdf (accessed 7.28.20).

Gawronek, P., Makuch, M., Mitka, B., and Gargula, T., (2019). Measurements of the Vertical Displacements of a Railway Bridge Using TLS Technology in the Context of the Upgrade of the Polish Railway Transport. *Sensors* ,19, 4275.

High Speed Two Limited (2017). High Speed Two Phase One C3 : Ground Settlement [WWW Document]. URL https://assets.publishing.service.gov.uk/government/uploads/system/uploads/attachment_data/file/672194/C3_-_Ground_Settlement__v1.pdf (accessed 7.28.20).

Jafari, B., Khaloo, A., and Lattanzi, D., (2017). Deformation Tracking in 3D Point Clouds Via Statistical Sampling of Direct Cloud-to-Cloud Distances. J. Nondestruct. Eval. 36, pp. 1-10.

Kersten, T.P., Lindstaedt, M., and Stange, M., (2021). Investigations into the geometric accuracy of latest terrestrial laser scanners in the laboratory and in the field. *AVN Allg. Vermessungs-Nachrichten*, 128, pp. 59–67.

Lague, D., Brodu, N., and Leroux, J., (2013). Accurate 3D comparison of complex topography with terrestrial laser scanner: Application to the Rangitikei canyon (N-Z). *ISPRS J. Photogramm. Remote Sens.*, 82, pp. 10–26.

Lazarus, D., and Jung, H. Il, (2018). Damage assessment and monitoring for buildings on the Elizabeth line. *Struct. Eng.* 96, pp. 14–24.

Mugnai, F., Lombardi, L., Tucci, G., Nocentini, M., Gigli, G., and Fanti, R., (2019). Geomatics in bridge structural health monitoring, integrating terrestrial laser scanning techniques and geotechnical inspections on a high value cultural heritage. *ISPRS Ann. Photogramm. Remote Sens. Spat. Inf. Sci*. 42, pp. 895–900.

Mukupa, W., Roberts, G.W., Hancock, C.M., and Al-Manasir, K., (2017). A review of the use of terrestrial laser scanning application for change detection and deformation monitoring of structures. *Surv. Rev*. 49, pp. 99–116.

Burland, J. B., Standing, J. R., and Jardine, F. M. (2001). *Building response to tunnelling. Case studies from construction of the jubilee line extension*. London, pp. 134-145.

VINCI Construction (2014). Crossrail C510 - Overview Crossrail C510 [WWW Document]. URL http://www.aftes.asso.fr/contenus/upload/File/Publications/Autres/2015-03-26/9-VGP - Crossrail-.pdf (accessed 7.9.20).

Wang, Q., and Kim, M.K., (2019). Applications of 3D point cloud data in the construction industry: A fifteen-year review from 2004 to 2018. *Adv. Eng. Informatics,* 39, pp. 306–319.